Effectiveness of termite hill as an economic adsorbent for the adsorption of alizarin red dye

Olushola S. Ayanda, Olusola S. Amodu, Habibat Adubiaro, Godwin O. Olutona, Oluwapese T. Ebenezer, Simphiwe M. Nelana and Eliazer B. Naidoo

ABSTRACT

The adsorption of alizarin red (AR) dye onto termite hill sample (THs) was investigated. Prior to the adsorption studies, the elemental, morphological, surface and structural properties of THs were examined by modern analytical methods. Instrumental analysis showed that the homogenous micro-structured THs are comprised of iron oxide, silica oxide, and alumina as major components. Experiments showed that the adsorption capacity of AR decreases with increasing pH and initial AR concentrations, and increases with increasing contact time, stirring speed and temperature. The equilibrium study obeyed the Langmuir adsorption model and the kinetics followed the pseudo-second-order model. About 95.0% AR reduction (1.425 mg/g) was achieved when 0.8 g of THs was mixed with 30 mL of 40 mg/L AR solution for 120 min at 400 rpm and a pH of 2. Thermodynamic study suggested that AR adsorption onto THs is spontaneous at higher temperatures of 323 K and above (ΔG^o values are negative). However, ΔG^o are positive at lower temperatures of 293–313 K, which implies that the adsorption process is not spontaneous at these temperatures. This study showed that THs could be used as alternative, low-cost, natural adsorbents for the removal of dyes from wastewater.

Key words | adsorption models, alizarin red dye, remediation process, termite mound, wastewater treatment

Olushola S. Ayanda (corresponding author)
Simphiwe M. Nelana
Eliazer B. Naidoo
Department of Chemistry,
Vaal University of Technology,
Vanderbijlpark 1900,
South Africa
E-mail: *osayanda@gmail.com*

Olushola S. Ayanda
Habibat Adubiaro
Oluwapese T. Ebenezer
Nanoscience Research, Department of Industrial Chemistry, Federal University Oye Ekiti,
P.M.B 373, Oye Ekiti, Ekiti State,
Nigeria

Olusola S. Amodu
Department of Chemical Engineering,
Lagos State Polytechnic,
P.M.B. 21606, Lagos,
Nigeria

Godwin O. Olutona
Department of Chemistry and Industrial Chemistry,
Bowen University, Osun State,
Nigeria

INTRODUCTION

In numerous industries, such as cosmetics, textiles, cotton, paper, plastics, leather, pharmaceuticals and food, dyes are used to colour the products (Afkhami & Moosavi 2010). Consequently, large amounts of coloured wastewater are generated. The presence of dyes in wastewaters raises tremendous concerns: the presence of dyes in water, even at very low concentration, might lead to reduction in the aesthetic value of water. The degradation by-products of some organic dyes are potentially toxic, carcinogenic, mutagenic and allergenic to marine life (Chung & Cerniglia 1992). Besides, the presence of these dyes in the environment may lead to collapse of some dyeing industries due to non-compliance with quality standards specified by the ISO 14000 certification. Alizarin is an anthraquinone originally derived from the root of the madder plant (Ghaedi *et al.* 2011). Synthetic dyes, such as Alizarin Red S (AR-S), belong to the most durable dyes; they cannot be completely degraded by general chemical, physical and biological processes

doi: 10.2166/wrd.2018.026

(Gautam *et al.* 2013). This is attributed to their complex aromatic structures, which give them physicochemical, thermal and optical stability. Different methods such as adsorption, coagulation, advanced oxidation, and membrane separation are used in the removal of dyes from wastewater (Gupta 2009).

Adsorption techniques have been a focus of significant research in recent years owing to their simplicity and high efficiency, as well as the availability of a wide range of adsorbents (Afkhami *et al.* 2008; Afkhami *et al.* 2009). Adsorbents such as activated carbon, zeolites, clay, nano-oxides and agricultural waste have been tested and used for the removal of dyes from polluted water (Allen *et al.* 2004; Crini 2006; Chakraborty *et al.* 2011; Ayanda *et al.* 2014; Amodu *et al.* 2015). Jadhava *et al.* 2011 studied the adsorption of AR-S onto nanocrystalline $Cu_{0.5}Zn_{0.5}Ce_3O_5$, and reported that the adsorption isotherms agreed with the Langmuir and Freundlich isotherm models, and that approximately 83.0% of AR-S was removed at lower temperature. Ramesh *et al.* (2016) studied the adsorption of AR dye onto calcium hydroxide as low-cost adsorbent. It was reported that calcium ions have very strong affinity and bind effectively to AR dye during staining of biomaterials. The authors also reported that the adsorption of AR dye on calcium hydroxide is endothermic and occurs spontaneously. It was stated that the adsorption process is effective at pH 12 (60 °C) and the kinetic parameters indicate that the adsorption phenomena is of monolayer type and fit well the pseudo-second-order rate equation.

Abdus-salam & Buhari (2014) studied the adsorption of AR dye onto activated carbon from mango seed; the adsorption of AR dye was described as rapid for the first 15 min of agitation with 86.90% removal, and the adsorption equilibrium was achieved in 90 min of agitation with 90.44% AR dye removal. The adsorption data fitted well to the pseudo-second-order kinetic models and Langmuir isotherm.

Furthermore, Ghaedi *et al.* 2011 used multi-walled carbon nanotubes as adsorbents for the kinetic and equilibrium study of the removal of AR-S. The use of activated carbon, nanomaterials and composites for the treatment of wastewater is relatively expensive when compared with natural adsorbents or wastes. Therefore, the exploration of readily available natural adsorbents that will effectively remediate wastewater with or without the initial treatment processes is necessary.

Termites are insects belonging to the Isoptera order, with around 2,800 species known worldwide (Araujo *et al.* 2013). Termite hills (THs) are built by mound-building termites that significantly modify the physicochemical properties of soil and have the ability to alter the mineralogy of the soil (Jouquet *et al.* 2002; Semhi *et al.* 2008). THs are built with soil particles and termite saliva in varying proportions and may reach up to 8 m in height and 15 m in width. They are ubiquitous and have been found to be rich in organic matter, silica and minerals such as iron and aluminium, etc. (Abe & Wakatsuki 2010; Abdus-Salam & Itiola 2012).

Extensive literature survey has shown the use of THs as natural adsorbent for the removal of heavy metals such as chromium, arsenic and excess fluoride in different environmental media (Araujo *et al.* 2013; Fufa *et al.* 2013; Fufa *et al.* 2014). However, THs have not been investigated for the removal of AR dye. In this report, we present the characterization of THs and their use as an alternative, low-cost natural adsorbent for the removal of AR dye from aqueous solution.

MATERIALS AND METHODS

Chemicals, termite hill samples, and instrumentation

AR (Figure 1) was purchased from PS Park Scientific Limited, Northampton, UK. Stock solution containing 1,000 mg/L AR dye was prepared by dissolving 1.0 g of AR dye in 1,000 mL of deionized water, and stored in the dark at 4 °C. Working solutions were prepared daily using serial dilution. The TH sample was mined at Oye-Ekiti, Ekiti

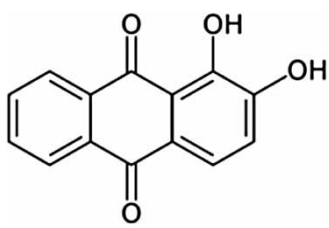

Figure 1 | Alizarin red dye.

State, Nigeria. The sample was air-dried in the laboratory at room temperature. The sample was placed in an oven at 60 °C for 3 hr before crushing and grinding in a mortar. It was sieved with a mesh of 0.5 mm pore size. The ash content, moisture content and the pH of the sample (in 50 mL distilled water) were carried out and reported elsewhere (Ayanda *et al.* 2017).

The elemental analysis of THs was determined qualitatively by the use of energy dispersive spectroscopy (EDS) attached to a scanning electron microscope (SEM; Nova Nano SEM 230); SEM and a transmission electron microscope (TEM; FEI Tecnai G^2 20) was used for the morphological studies; XRF analysis was carried out by the Skyray Instrument EDX3600B X-ray fluorescence spectrometer; while attenuated-total-reflection–Fourier-transform-infrared spectroscopy (ATR–FTIR) was used for clarification of the structural properties of THs. The Brunauer, Emmett and Teller (BET) surface area of THs was obtained by the use of a TriStar 3,000 analyzer with N_2 adsorption at −196 °C. THs samples were first degassed at 200 °C for 4 h prior to the analysis.

Adsorption procedure

To investigate the effect of THs dosage, a range of THs (0.125–1.5 g) were mixed in a conical flask with 30 mL of 40 mg/L AR dye and stirred with a magnetic stirrer at 200 rpm for 20 min. For the effect of the initial concentration, 30 mL sample solutions of AR dye with concentrations ranging from 20 to 200 mg/L were mixed with 0.8 g THs in a conical flask and stirred at 200 rpm for 20 min. The data obtained on the effect of initial AR concentration were used for the equilibrium studies. To examine the effect of contact time, 0.8 g THs was mixed with 30 mL of 40 mg/L AR dye solution in a conical flask and stirred for different contact times ranging from 20 to 120 min at 200 rpm. The data obtained on the effect of contact time were used for the kinetic studies. The effect of pH was considered by the addition of 30 mL of 40 mg/L AR dye solutions into a conical flask with the pH adjusted with 0.01 M HCl and NaOH at pH values ranging from 2 to 12; 0.8 g of THs was added and stirred for 20 min at 200 rpm. Moreover, samples of 0.8 g THs were agitated with 30 mL of 40 mg/L AR dye solution and placed in a conical flask for 20 min at 200 rpm to study the effect of temperature; the temperatures considered ranged from 293 K to 338 K. The data obtained on the effect of temperature were used for the thermodynamic studies. Lastly, to study the effect of stirring speed, 30 mL solution of 40 mg/L AR dye and a constant 0.8 g THs were placed in a conical flask and stirred for 20 min. A range of stirring speeds (100–400 rpm) was investigated.

After each of the experiments, an aliquot was withdrawn and a UV/visible spectrophotometer was used to determine the concentration of AR ($\lambda_{max} = 450$ nm). The percentage AR dye removal was calculated with Equation (1) and the amount of AR dye adsorbed (q_e; *mg* of AR dye per *g* THs) was calculated using Equation (2).

$$\% \text{ Removal} = \frac{C_o - C_e}{C_o} \times 100 \tag{1}$$

$$q_e = \frac{C_o - C_e}{W} \times V \tag{2}$$

where C_o and C_e (mg/L) are the initial and equilibrium concentrations of the AR dye solution, respectively, V (mL) is the volume of the solution and W (g) is the mass of THs used.

Kinetic, equilibrium and thermodynamics models

The linearized form of the pseudo-first- and pseudo-second-order kinetic models are presented in Equations (3) and (4), respectively.

$$\log_{10}(q_e - q_t) = \log q_e + \frac{k_1}{2.303} t \tag{3}$$

$$\frac{t}{q_t} = \frac{1}{k_2 q_e^2} + \frac{t}{q_e} \tag{4}$$

where q_e is the equilibrium amount of AR dye adsorbed per unit mass of THs (mg/g), q_t is the amount of AR dye adsorbed per unit mass of THs at time t (mg/g), k_1 and k_2 are the pseudo-first- and pseudo-second-order adsorption rate constants, respectively, and t is time (min).

For the adsorption process obeying the pseudo-first-order kinetic model, a plot of $\log_{10}(q_e - q_t)$ against t will

give a straight line graph with the q_e (mg/g) and k_1 obtained from the intercept and slope of the graph (Equation (3)), respectively. However, a straight line graph of a plot of t/q_t against time t (Equation (4)) is an indication that the adsorption process follows the pseudo-second-order kinetic model, and k_2 and q_e (mg/g) are calculated from the intercept and slope of the plot, respectively.

The linearized form of the Langmuir (1918) and Freundlich (1907) models are presented in Equations (5) and (6), respectively.

$$\frac{1}{q_e} = \frac{1}{q_m K_L} \cdot \frac{1}{C_e} + \frac{1}{q_m} \tag{5}$$

$$\log_{10} q_e = \log_{10} K_F + \frac{1}{n} \log_{10} C_e \tag{6}$$

where C_e, q_e, q_m and n are the equilibrium concentration of AR dye solution (mg/L), amount of AR dye adsorbed per unit mass of THs (mg/g), maximum amount of AR dye adsorbed per unit mass of THs (mg/g) and Freundlich model constant indicating intensity of adsorption, respectively. K_L and K_F are the Langmuir constant representing energy of adsorption (L/mg) and the Freundlich constant (mg/g (L/mg)$^{1/n}$), respectively.

A plot of C_e/q_e against C_e will be linear for an adsorption process obeying the Langmuir model with q_m and K_L calculated from the slope and intercept, respectively. The main features of the Langmuir isotherm are usually expressed by the dimensionless separation factor (R_L) given as Equation (7). An isotherm is favourable if $0 < R_L < 1$; unfavourable if $R_L < 1$; linear if $R_L = 1$ and irreversible if $R_L = 0$.

$$R_L = \frac{1}{1 + k_L C_o} \tag{7}$$

Conversely, for an adsorption process obeying the Freundlich isotherm, the plot of $\log_{10} q_e$ against $\log_{10} C_e$ will be linear with K_F and n obtained from the intercept and slope, respectively. A value of n between 1 and 10 indicates a favourable adsorption process.

The standard free energy (ΔG^o), enthalpy (ΔH^o) and entropy (ΔS^o) changes were calculated from thermodynamic equations presented in Equations (8)–(10) (see Ayanda *et al.* 2015).

$$\Delta G^0 = -RT \ln K \tag{8}$$

$$K = \frac{C_o - C_e}{C_e} \tag{9}$$

$$\log K = \frac{\Delta S^o}{2.303R} - \frac{\Delta H^o}{2.303RT} \tag{10}$$

where $C_o - C_e$ is the amount of the AR dye adsorbed per litre, C_e is the equilibrium concentration of solution in mg/L, T is temperature in Kelvin (K), R is the ideal gas constant (8.314 J/mol/K) and K is the thermodynamic equilibrium constant. A plot of $\log K$ against $1/T$ gave ΔH^o and ΔS^o from the slope and intercept of Equation (10), respectively.

RESULTS AND DISCUSSION

SEM and TEM analyses of THs

A homogeneous microstructure of THs by SEM is presented in Figure 2(a). According to Millogo *et al.* (2011), THs consist of a homogeneous microstructure of big quartz grains connected by irregular kaolinite particles. Moreover, the TEM image (Figure 2(b)) showed that THs consist of crystalline sheet-like particles of different shapes. The TEM is supported by Ganguli *et al.* 2014 who reported that the TEM image of THs showed sheet- and rod-like morphology of α-quartz silica.

Elemental investigation of THs

The EDS spectrum of THs is as shown in Figure 3. The estimated percentage composition of elements in the THs by EDS is C (20.44 ± 1.74 wt%), O (59.99 ± 2.58 wt%), Al (7.92 ± 2.55 wt%), and Si (11.66 ± 3.05 wt%). This method of analysis is not an accurate analytical technique to quantitatively determine the chemical composition of samples, thus, the quantitative elemental composition was carried out by XRF.

It was observed according to the XRF analysis of THs presented in Table 1 that iron oxide (23.8 wt %) is the

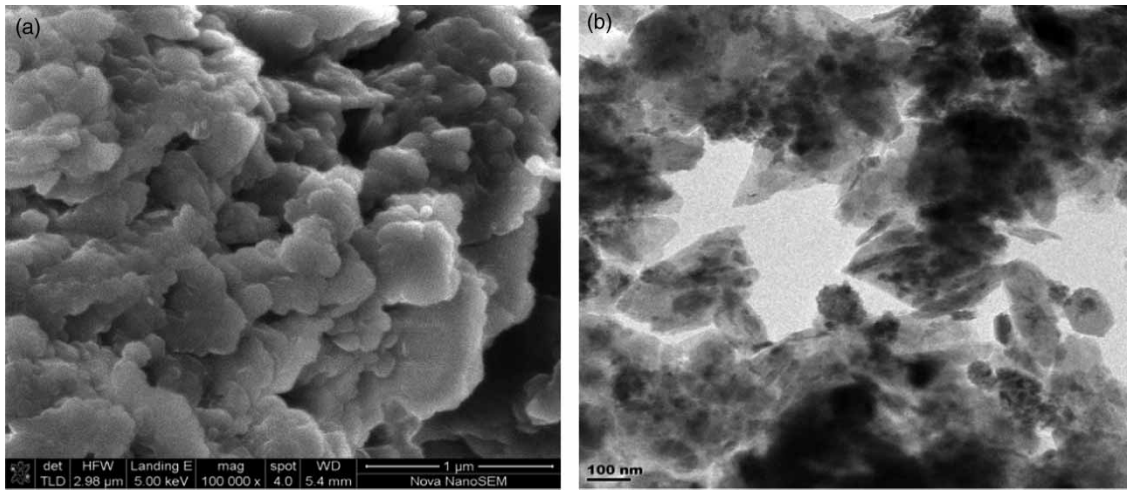

Figure 2 | SEM (a) and TEM (b) images of termite hills.

most abundant component, followed by silica oxide (20.6 wt %) and alumina (14.4 wt %). The compositions of Fe, Si, and Al sum up to 58.83 wt%; Mg, As, Au, Ag and Cd were absent. The highest percentage of Fe in THs might be due to the presence of montmorillonite clay minerals (Wanyika *et al.* 2016), moreover, the presence of Fe might explain the reddish-brown colouration of THs. The mineral phases of the THs as verified by X-ray diffraction (Ayanda *et al.* 2017) are kaolinite and quartz.

FTIR examination

As shown in Figure 4, the wavenumbers 3,620.51 cm^{-1} and 3,693.04 cm^{-1} are typical absorption bands for kaolin (Saikia & Parthasarathy 2010). The band at 3,620.51 cm^{-1} shows the presence of inner hydroxyls in the THs while the bands at 3,693.04 cm^{-1} could be assigned to Al–OH or Si–OH stretching. Bands at 1,002.85 cm^{-1} and 910.49 cm^{-1} could be assigned to Si–O stretching, the wavenumbers 752.07 cm^{-1} and 792.41 cm^{-1} shows the presence of Si–O quartz, whereas the band at 683.91 cm^{-1} could be assigned to Si–O–Si bending in the THs.

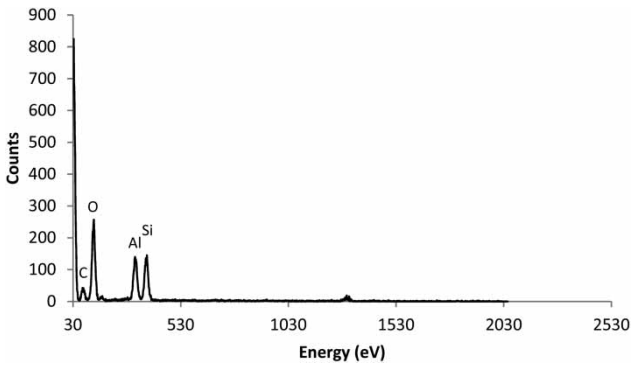

Figure 3 | EDS spectrum of termite hills.

The BET surface area of THs was recorded as 35.36 m^2/g; this is higher than the surface area of the uncalcinated THs (28.40 m^2/g) reported by Fufa (2016). The difference in the surface area might be due to differences in the sizes of the THs particles resulting from different methods of sample preparation. As expected, the BET surface area of treated or calcined THs will be higher.

Adsorption results

Effect of adsorbent dosage and initial concentration

The results of the effect of THs dosage on the adsorption of 40 mg/L AR dye are shown in Figure 5. The results showed that an increase of the THs dosage from 0.125 g to 0.5 g increases the percentage of AR dye removal from 22.5% to 45.0% at a contact time of 20 min. The increase in the percentage of the removed AR dye might be due to increase in the number of active sites of the THs as the dose increases. Equilibration was attained at 0.8–1.0 g, after which the percentage of AR dye removed slightly decreased. The trend of the graph is similar to the results obtained by

Table 1 | Chemical composition of termite hills

Element	Content (wt%)
Mg	0.0000
Al	14.4332
Si	20.6140
P	0.1474
S	0.3106
K	0.7585
Ca	0.1074
Ti	0.7040
V	0.0260
Cr	0.0272
Mn	0.1389
Co	0.2622
Fe	23.7794
Ni	0.0762
Cu	0.0499
Zn	0.0876
As	0.0000
Pb	0.0127
W	0.0305
Au	0.0000
Ag	0.0000
Rb	0.0128
Nb	0.0068
Mo	0.2055
Cd	0.0000
Sn	0.8308
Sb	0.7187

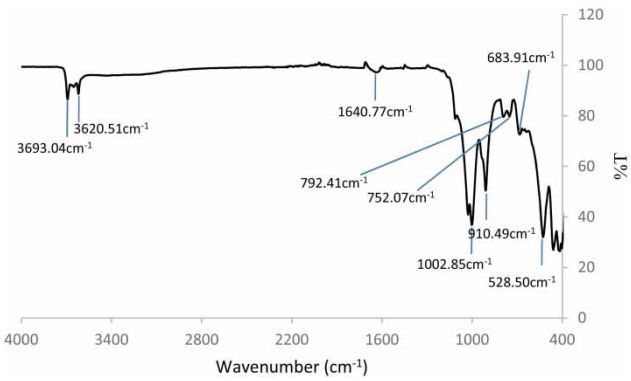

Figure 4 | FTIR spectrum of termite hills.

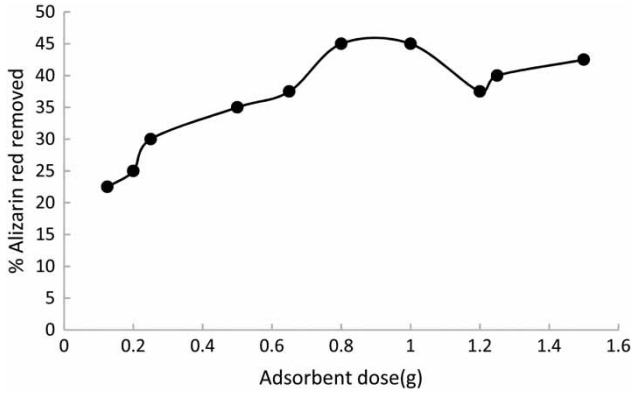

Figure 5 | Effect of termite hills dosage on the adsorption of alizarin red dye.

Sujitha & Ravindhranath (2016) and the maximum percentage removal (45.0%) makes 0.8 g and 1.0 g as a potential usage in the experiment, but 0.8 g was preferred due to low consumption of THs.

The effect of initial AR concentration on the adsorption of AR dye onto THs is as presented in Figure 6. The figure shows that the percentage removal of AR dye decreases as the initial concentration increases; approximately 55.0% AR dye removal was achieved by mixing 30 mL of 20 mg/L AR dye with 0.8 g THs for 20 min at 200 rpm, whereas 17.0% was achieved for 200 mg/L AR dye solution. This implies that the adsorption process depends on the initial dye concentration. At lower initial concentrations, the concentration of the dye provides the necessary driving force to overcome the resistance to the mass transfer of the dye molecules between the aqueous phase and the solid phase. This enhances the uptake of AR dye molecule from the aqueous phase onto the THs. There was a decrease in the percentage of AR dye removal since

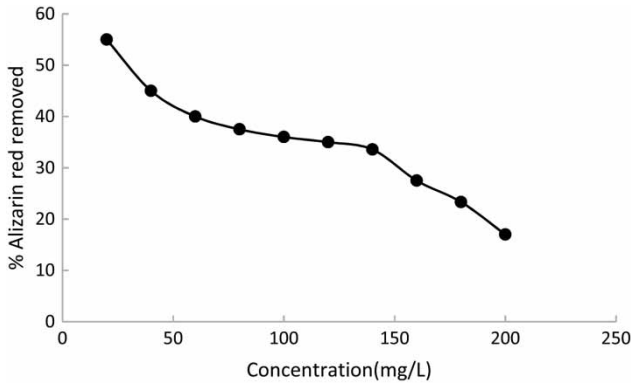

Figure 6 | Effect of initial concentration on the adsorption of alizarin red dye onto termite hills.

the adsorption was carried out against a fixed number of active sites (Sujitha & Ravindhranath, 2016).

Effect of pH and temperature on AR dye adsorption

It was observed from Figure 7 that the percentage of AR dye removal also decreases with increase in the pH of the solution. About 60.0% removal was possible at pH 2, decreasing to about 30.0% at pH 12. Thus, it could be inferred that acidic conditions favour the adsorption of AR dye onto THs. AR dye is yellowish in colour under acidic conditions and looks clearer when treated with THs. This behaviour could be attributed to the anionic nature of the AR dye. As the pH decreases, the surface of the THs is positively charged and subsequently the surface has affinity towards negatively charged species of the AR dye.

The effect of temperature on AR dye adsorption onto THs was studied at temperatures ranging from 293 K to 339 K. It was observed that the higher removal due to increasing temperature (Figure 8) may be attributed to an increase in the mobility of the AR dye molecules. The increase in the percentage of AR dye adsorbed from 37.5% to 57.5% with increasing temperature may suggest an increasing accessibility of the AR dye molecules to the THs active sites. Thus, the adsorption process is endothermic.

Effect of contact time and stirring speed on AR dye adsorption

It was observed from Figure 9 that the percentage removal of the AR dye increases from 45.0% (0.68 mg/g) to 60.0% (0.90 mg/g) with increase in the contact time from 20 min

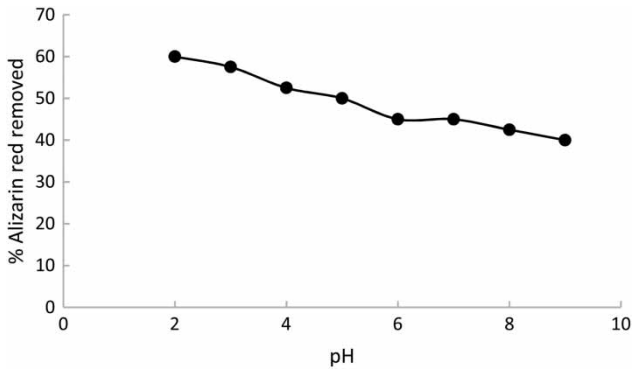

Figure 7 | Effect of pH on the adsorption of alizarin red dye onto termite hills.

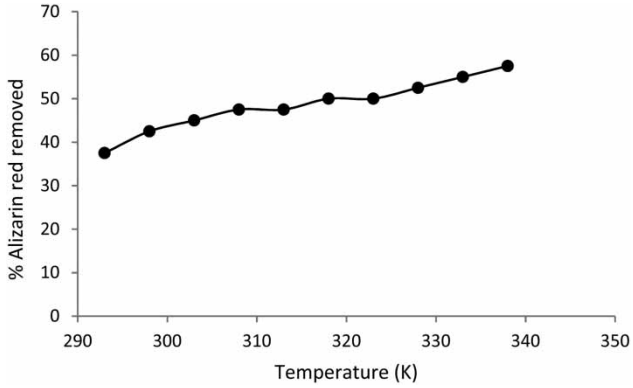

Figure 8 | Effect of temperature on the adsorption of alizarin red dye onto termite hills.

to 120 min, respectively. This is supported by Ramesh *et al.* (2016) who reported that the adsorption equilibrium of AR dye onto calcium hydroxide was attained after 120 min. This may be attributed to the fact that a larger surface area of the THs is being made available with time for the adsorption of AR dye molecules. The data obtained on the effect of contact time play an important role in the analysis of the kinetic study of adsorption.

Figure 10 shows the result of the effect of stirring speed on the adsorption of AR dye; it was observed that as the stirring speed increases, the percentage removal also increases from 40.0% to 52.5% at 100 to 400 rpm. This implies that the speed also plays a vital role on the active site of THs and AR dye concentration. The trend is similar to the work reported by Raut *et al.* (2012).

Isotherm, kinetic and thermodynamic studies

The Langmuir isotherm is used to determine whether the adsorption process occurs through a monolayer formation.

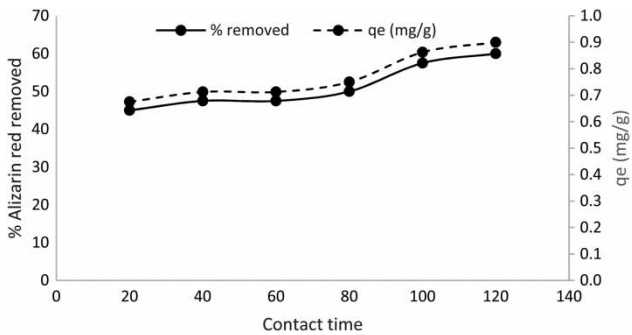

Figure 9 | Effect of contact time on the adsorption of alizarin red dye onto termite hills.

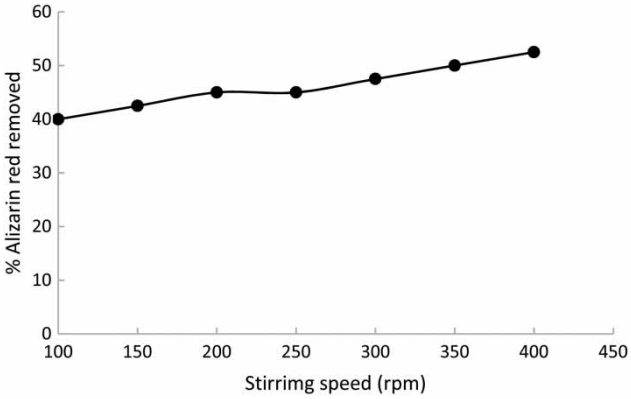

Figure 10 | Effect of stirring speed on the adsorption of alizarin red dye onto termite hills.

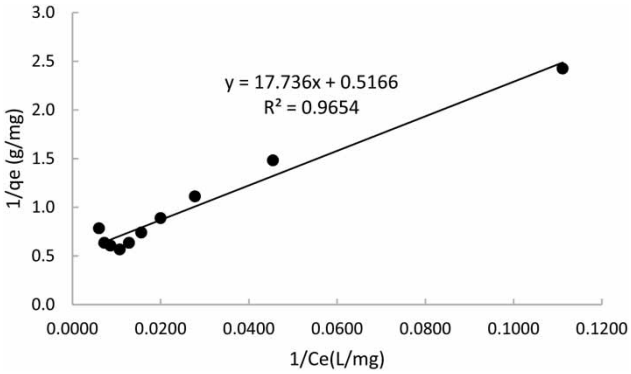

Figure 11 | Langmuir isotherm of alizarin red dye adsorption onto termite hills.

The regression coefficient ($R^2 = 0.9654$) obtained for the Langmuir plot (Figure 11) confirms that the adsorption process matches the Langmuir adsorption model. The Langmuir monolayer adsorption constant, q_m (mg/g) and Langmuir energy of adsorption constant, K_L are presented in Table 2.

The relation between R_L and C_o to represent the features of the Langmuir isotherm for THs is shown in Figure 12. The R_L for the initial AR concentrations are found in the range 0.00015–0.0015 which suggests a favourable adsorption of AR dye onto THs under the conditions of the experiment.

The Freundlich isotherm assumes that the dye uptake occurs on a heterogeneous surface by multilayer adsorption and that the amount of the adsorbed adsorbate increases with an increase in adsorbate concentration. The equilibrium adsorption plot shows that AR dye adsorption onto THs does not suit the Freundlich isotherm due to the low regression coefficient value of 0.8573 (Figure 13). K_F and n obtained are also presented in Table 2.

The pseudo-first-order and pseudo-second-order kinetics as tested on the adsorption of AR dye onto THs are presented in Figures 14 and 15, respectively. The adsorption kinetics followed the pseudo-second-order equation, having a higher regression coefficient value of 0.9729; this showed that chemisorption is the main rate limiting step. Table 2 also presents the calculated kinetic parameters and regression coefficient.

The van 't Hoff plot for the adsorption of AR dye onto THs is as presented in Figure 16. The calculated ΔG^o, ΔH^o and ΔS^o for the THs are given in Table 3. The negative value of ΔG^o shows that the adsorption process is spontaneous at 323 K and above, but non-spontaneous at lower temperatures of 293 K to 318 K. The positive value of ΔH^o (13.016 kJ/mol) also affirms that the adsorption process is endothermic.

Table 2 | Isotherm and kinetic parameters for alizarin red dye adsorption onto termite hills

Isotherm					
Langmuir model			**Freundlich model**		
q_m (mg/g)	K_L (L/mg)	R^2	K_F (mg/g (L/mg)$^{1/n}$)	n	R^2
0.0564	34.32	0.9654	0.1634	2.0978	0.8573
Kinetic models					
Pseudo-first-order			**Pseudo-second-order**		
k_1(min^{-1})	q_e(mg/g)	R^2	k_2(g/mg/min)	q_e(mg/g)	R^2
−0.0237	0.5919	0.7916	0.06782	0.9717	0.9729

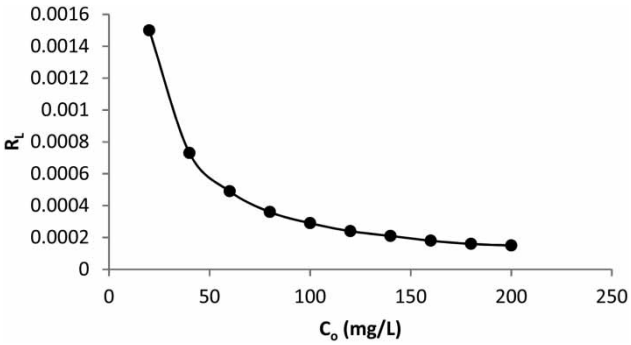

Figure 12 | Plot of R_L versus initial alizarin red dye concentration.

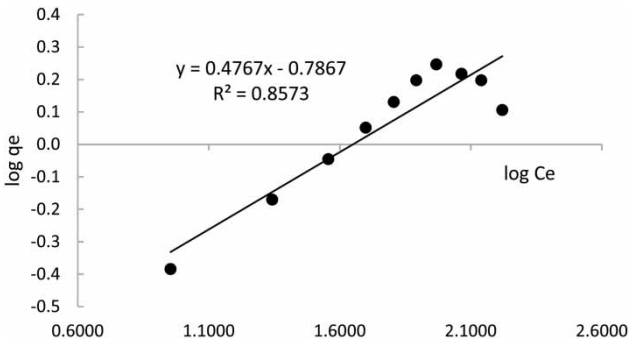

Figure 13 | Freundlich isotherm of alizarin red dye adsorption onto termite hills.

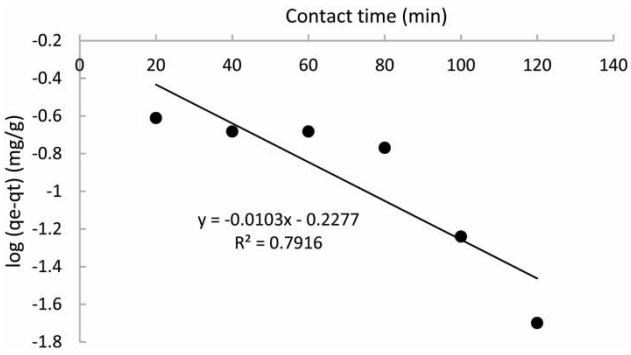

Figure 14 | Pseudo-first-order kinetic plot.

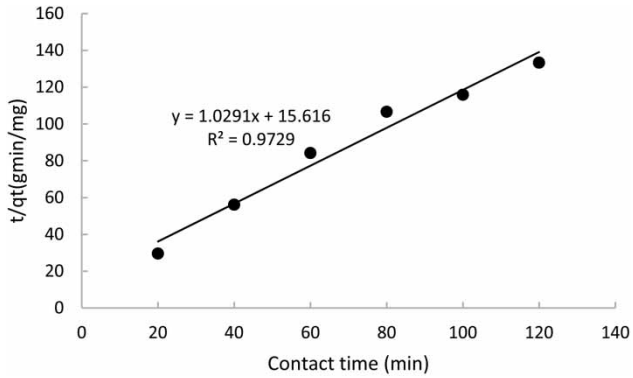

Figure 15 | Pseudo-second-order kinetic plot.

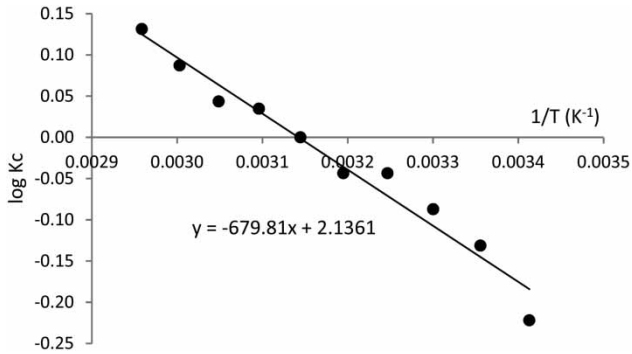

Figure 16 | Van 't Hoff plot.

Table 3 | Thermodynamic parameters of alizarin red dye adsorption onto termite hills

T (K)	ΔH^o kJ/mol	ΔS^o J/mol/K	ΔG^o J/mol
293	13.016	40.9	1,244.4
298			748.9
303			505.5
308			256.3
313			260.4
318			0.0
323			−214.9
328			−272.9
333			−555.6
338			−849.4

All optimal conditions were chosen (THs dosage, 0.8 g; pH 2; contact time, 120 min; stirring speed, 400 rpm) and applied to the treatment of 40 mg/L AR dye solution at ambient temperature. The result showed that approximately 95.0% AR dye removal was achieved when 30 mL of 40 mg/L AR dye was contacted with 0.8 g THs for 120 min at pH 2 and stirring speed of 400 rpm. A comparison of the amount of AR dye removed by different adsorbents is listed in Table 4. The percentage of AR dye removed by THs demonstrated in this study shows satisfactory performance in comparison with other adsorbents in the literature.

Table 4 | Comparison of the amount of alizarin red dye removed

Adsorbents	Amount of AR removed	Reference
$Cu_{0.5}Zn_{0.5}Ce_3O_5$	83.0%	Jadhava *et al.* (2011)
Mango seed activated carbon	90.44%	Abdus-Salam & Buhari (2014)
Activated charcoal	8.97 mg/g	Ishaq *et al.* (2014)
Walnut shell activated carbon	18.05 mg/g	Savran *et al.* (2014)
Lantana camara biosorbent	1.17 mg/g	Gautam *et al.* (2014)
Achyranthes aspera carbon	89%	Sujitha & Ravindhranath (2016)
Chitosan/ZnO nanorods composite	8.01 mg/g	Ali & Mohamed (2017)
Termite hill	95.0%	This study

CONCLUSION

The ability of THs to remove AR dye from simulated AR dye solution was investigated. The present study has shown that THs will serve as low-cost adsorbent for the removal of AR dye from contaminated wastewater. The homogeneous microstructured THs is comprised of iron oxide, silica oxide, and alumina, with a BET surface area of 35.36 m^2/g. Experimental results showed that the removal of AR dye increases with increase in the THs dosage, contact time, stirring speed and temperature, but decreases with increase in pH and initial AR dye concentrations. The adsorption obeyed the Langmuir adsorption model, while the adsorption kinetics followed the pseudo-second-order equation. The thermodynamic parameters showed that the adsorption process is endothermic and spontaneous at 323 K and above. Thus, AR adsorption onto THs has good feasibility as a process at high temperature. The effectiveness of THs for the removal of AR dye (95.0% AR removal) may be credited to the elemental composition of THs, such as the presence of Fe, Si and Al oxides. The treatment of real dye wastewater with THs will be carried out in future to compare the results with the simulated dye solution, as the presence of additives may affect the efficiency of adsorption.

ACKNOWLEDGEMENTS

We acknowledge Miranda Waldron of the Electron Microscope Unit, University of Cape Town for the SEM and TEM analysis of the termite hill sample.

REFERENCES

Abdus-Salam, N. & Buhari, M. 2014 Adsorption of alizarin and fluorescein dyes on adsorbent prepared from mango seed. *Pacific Journal of Science and Technology* **15**, 232–244.

Abdus-Salam, N. & Itiola, A. D. 2012 Potential application of termite mound for adsorption and removal of Pb(II) from aqueous solutions. *Journal of Iran Chemical Society* **9**, 373–382.

Abe, S. S. & Wakatsuki, T. 2010 Possible influence of termites (*Macrotermes bellicosus*) on forms and composition of free sesquioxides in tropical soils. *Pedobiologia* **53**, 301–306.

Afkhami, A. & Moosavi, R. 2010 Adsorptive removal of Congo red, a carcinogenic textile dye, from aqueous solutions by maghemite nanoparticles. *Journal of Hazardous Materials* **174**, 398–403.

Afkhami, A., Madrakian, T., Amini, A. & Karimi, Z. 2008 Effect of the impregnation of carbon cloth with ethylenediaminetetraacetic acid on its adsorption capacity for the adsorption of several metal ions. *Journal of Hazardous Materials* **150**, 408–412.

Afkhami, A., Madrakian, T. & Amini, A. 2009 Mo(VI) and W(VI) removal from water samples by acid-treated high-area carbon cloth. *Desalination* **243**, 258–264.

Ali, O. & Mohamed, S. 2017 Adsorption of copper ions and alizarin red S from aqueous solutions onto a polymeric nanocomposite in single and binary systems. *Turkish Journal of Chemistry* **41**, 967–986.

Allen, S. J., McKay, G. & Porter, J. F. 2004 Adsorption isotherm models for basic dye adsorption by peat in single and binary component systems. *Journal of Colloid and Interface Science* **280**, 322–333.

Amodu, O. S., Ojumu, T. V., Ntwampe, S. K. & Ayanda, O. S. 2015 Rapid adsorption of crystal violet onto magnetic zeolite synthesized from fly ash and magnetite nanoparticles. *Journal of Encapsulation and Adsorption Sciences* **5**, 191–203.

Araujo, R. R., Reis, J. O. M., Rezende, E. I. P., Mangrich, A. S., Wisniewski Jr., A., Dick, D. P. & Romao, L. P. C. 2013 Application of termite nest for adsorption of Cr(VI). *Journal of Environmental Management* **129**, 216–223.

Ayanda, O. S., Fatoki, O. S., Adekola, F. A., Petrik, L. F. & Ximba, B. J. 2014 Application of nano zinc oxide (nZnO) for the removal of triphenyltin chloride (TPT) from dockyard wastewater. *Water SA* **40**, 659–664.

Ayanda, O. S., Fatoki, O. S., Adekola, F. A., Ximba, B. J., Akinsoji, O. S. & Petrik, L. F. 2015 Coal fly ash supported nZnO for the sorption of triphenyltin chloride. *Archives of Environmental Protection* **41**, 63–75.

Ayanda, O. S., Odo, E. A., Malomo, D., Sodeinde, K. O., Lawal, O. S., Ebenezer, O. T., Nelana, S. M. & Naidoo, E. B. 2017 Accelerated decolorization of Congo red by powdered termite mound. *Clean Soil Air and Water* **45**, 1700537.

Chakraborty, S., Chowdhury, S. & Saha, P. D. 2011 Adsorption of crystal violet from aqueous solution onto NaOH-modified rice husk. *Carbohydrate Polymer* **86**, 1533–1541.

Chung, K. T. & Cerniglia, C. E. 1992 Mutagenicity of azo dyes: structure–activity relationship. *Mutation Research* **77**, 201–220.

Crini, G. 2006 Non-conventional low-cost adsorbents for dye removal: a review. *Bioresource Technology* **97**, 1061–1085.

Freundlich, H. 1907 Über die Adsorption in Lösungen [On adsorption in solutions]. *Zeitschrift für Physikalische Chemie* **57**, 385–470.

Fufa, F. 2016 Experimental evaluation of activated termite mound for fluoride adsorption. *IOSR Journal of Environmental Science, Toxicology and Food Technology* **10** (8), 119–132.

Fufa, F., Alemayehu, E. & Lennartz, B. 2013 Defluoridation of ground water using termite mound. *Water Air Soil Pollution* **224**, 1552–1567.

Fufa, F., Alemayehu, E. & Lennartz, B. 2014 Sorptive removal of arsenate using termite mound. *Journal of Environmental Management* **132**, 188–196.

Ganguli, A. K., Kumar, S., Baruah, A. & Vaidya, S. 2014 Nanocrystalline silica from termite mounds. *Current Science* **106**, 83–88.

Gautam, R. K., Mudhoo, A. & Chattopadhyaya, M. C. 2013 Kinetic, equilibrium, thermodynamic studies and spectroscopic analysis of Alizarin Red S removal by mustard husk. *Journal of Environmental Chemical Engineering* **1**, 1283–1291.

Gautam, R. K., Gautam, P. K., Chattopadhyaya, M. C. & Pandey, J. D. 2014 Adsorption of Alizarin Red S onto biosorbent of *Lantana camara*: kinetic, equilibrium modeling and thermodynamic studies. *Proceedings of National Academy of Sciences of India, Section A: Physical Sciences* **84**, 495–504.

Ghaedi, M., Hassanzadeh, A. & Nasirikokhdan, S. 2011 Multi-walled carbon nanotubes as adsorbents for the kinetic and equilibrium study of alizarin red S and morin. *Journal of Chemical and Engineering Data* **56**, 2511–2520.

Gupta, V. 2009 Application of low-cost adsorbents for dye removal – a review. *Journal of Environmental Management* **90**, 2313–2342.

Ishaq, M., Saeed, K., Shoukat, A., Ahmad, I. & Khan, A. R. 2014 Adsorption of alizarin red dye from aqueous solution on an activated charcoal. *International Journal of Science Inventions Today* **3**, 705–718.

Jadhava, H. V., Khetre, S. M. & Bamane, S. R. 2011 Removal of alizarin red-S from aqueous solution by adsorption on nanocrystalline $Cu_{0.5}Zn_{0.5}Ce_3O_5$. *Pelagia Research Library Der Chemica Sinica* **2**, 68–75.

Jouquet, P., Mamou, L., Lepage, M. & Velde, B. 2002 Effects of termites on clay minerals in tropical soils: fungus growing termites as weathering agents. *European Journal of Soil Science* **53**, 521–528.

Langmuir, I. 1918 The adsorption of gases on plane surfaces of glass, mica and platinum. *Journal of the American Chemical Society* **40**, 1361–1403.

Millogo, Y., Hajjaji, M. & Morel, J. C. 2011 Microstructure, physical and mechanical properties of clayey material from termite mound: a stabilized material for adobe building. *Applied Clay Science* **51**, 160–164.

Ramesh, T. N., Ashwini, A. & Kirana, D. V. 2016 Removal of alizarin red dye using calcium hydroxide as a low-cost adsorbent. *Journal of Applied Chemical Research* **10**, 35–47.

Raut, P. A., Dutta, M., Sengupta, S. & Basu, J. K. 2012 Alumina-carbon composite as an effective adsorbent for removal of methylene blue and alizarin red-s from aqueous solution. *Indian Journal of Chemical Technology* **20**, 15–20.

Saikia, B. J. & Parthasarathy, G. 2010 Fourier transform infrared spectroscopic characterization of kaolinite from Assam and Meghalaya, Northeastern India. *Journal of Modern Physics* **1**, 206–210.

Savran, A., Kul, A. R., Kubilay, S. & Gözeten, I. 2014 Removal of alizarin red S from aqueous solutions by adsorption using activated carbons prepared from walnut shell. *Journal of International Environmental Applications and Science* **9**, 648–656.

Semhi, K., Chaudhuri, S., Clauer, N. & Boeglin, J. L. 2008 Impact of termite activity on soil environment: a perspective from their soluble chemical components. *International Journal of Environmental Science and Technology* **4**, 431–444.

Sujitha, R. & Ravindhranath, K. 2016 Extraction of anionic dye, alizarin red S, from industrial waste waters using active carbon derived from the stems of *Achyranthes aspera* plant as bio-adsorbent. *Der Pharma Chemica* **8** (9), 63–73.

Wanyika, H., Maina, E., Gachanja, A. & Marika, D. 2016 Instrumental characterization of montmorillonite clays by X-ray fluorescence spectroscopy, Fourier transform infrared spectroscopy, X-ray diffraction and UV/visible spectrophotometry. *Journal of Agriculture, Science and Technology* **17**, 224–239.

First received 28 April 2018; accepted in revised form 30 July 2018. Available online 24 September 2018